Sensors & Transducers, Vol. 258, Issue 4, July 2022, pp. 25-30

Sensors & Transducers

Published by IFSA Publishing, S. L., 2022
http://www.sensorsportal.com

Preflight Preparations for Active Debris Removal and Ranging

[1] * Claude PHIPPS and [2] Christophe BONNAL
[1] Photonic Associates, LLC, 200A Ojo de la Vaca, Santa Fe, NM 87508, USA
[2] CNES, 52 rue Jacques Hilairet, 75612 Paris Cedex, France
[1] Tel.: +1-215-358-4360, fax: +1-505-466-3877
E-mail: crphipps@aol.com

Received: 8 June 2022 /Accepted: 15 July 2022 /Published:29 July 2022

Abstract: In this paper we present three technical improvements that will better prepare satellites for their later removal prior to launch, in accordance with international agreements such as the IADC Space Debris Mitigation Guidelines, which ensure that satellites are designed to re-enter within 25 years. Space debris are non-functional satellites orbiting the Earth, such as abandoned second stage rockets, nanosatellites (most of which have no onboard propulsion) and collision fragments including those from deliberate destruction. Just-in-time Collision Avoidance (JCA) can prevent anticipated collisions. It requires far more precise orbit parameters for debris than we have now. The main tool we will use is ultra-precise laser ranging from an orbiting ranging station, which can operate up to 500 km range from a debris, provided it has good optical cross-sections. To enhance cross-sections, we would install 1-cm optical corner reflectors on each satellite, four around its equator and two at its poles so that one or more will always be visible. We compare pulsed and frequency-chirped CW lasers in this regard. To better optimize energetic efficiency of laser propulsion to nudge satellites away from a predicted collision, we suggest the Thomson scattering technique, which permits simultaneously measuring the change of target velocity and the plume exhaust velocity, which can be combined to calculate this efficiency in real time.

Keywords: Laser ranging, Just in time collision avoidance, Picosecond laser, Thomson scattering, Chirped-frequency CW laser.

1. Introduction

We have discussed laser Active Debris Removal (ADR) extensively, including precise ranging[1,2] sufficient to reduce false collision alarms from 100/year to 0.02/year. In those works, we assumed the laser pulse originating from a spaceborne laser station scatters off a target satellite into PI steradians. At 1000 km range, the ranging system needed a 50 mJ, 100 ps pulsed laser and 75cm diameter optical aperture to attain adequate signal to noise (S/N) ratio. In this paper, we discuss prelaunch satellite modifications that can permit low power CW lasers to be used for ranging. A second (high power) pulsed laser is needed for the ultimate ”laser nudging” operation to prevent subsequent predicted collisions.

We propose three simple improvements in procedure to better prepare satellites for ADR at end of life if they become derelicts unable to re-enter themselves. These are enhancing satellite laser signal cross section and attaching special thrust plates to improve thrust direction control in “nudging,”[2] prior to launch, and implementing measurement of shot-to-shot kinetic efficiency during nudging. We also discuss ways to optimize ablation kinetic efficiency and to select optimum ablation fuels that could withstand millions rather than thousands of shots.

2. Pre-launch Preparation

2.1. Corner Reflectors

We can enhance laser signal cross section for easier Just-in-Time Collision Avoidance activities (JCA) by installing as few as six small corner reflectors (not refractive corner cubes) on the satellite surface.

A single 1-cm open corner reflector (Fig. 1) provides 4.4×10^{11} increase in brightness of the ranging laser return, compared to a simple rough metal surface scattering into PI steradians. Four around the satellite equator and two at the poles will suffice because a corner reflector has a 90-degree field of view (FOV) [4].

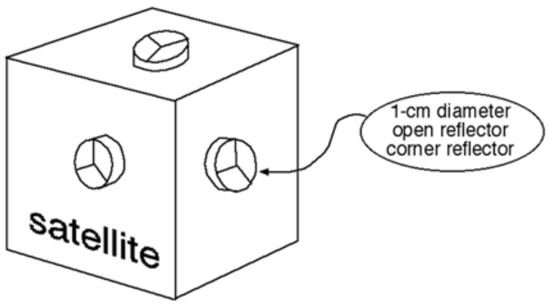

Fig. 1. Small corner reflectors on a satellite.

Corner cubes have smaller FOV. To achieve even greater brightness, a 10-cm patch of corner reflectors could be installed if it will not interfere with satellite operation (Fig. 2).

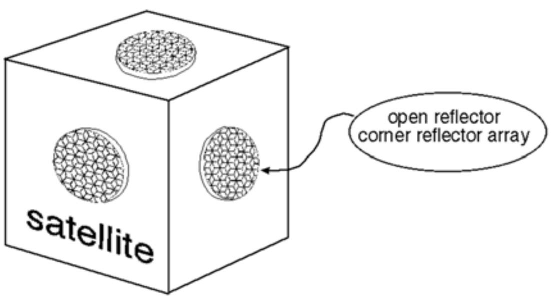

Fig. 2. Larger reflector patches on satellite.

Patches you see on highway signs are deliberately broadened and less bright, but we've all seen how effective they are. The post-Newtonian corrections due to Gambi [5, 6] must still be observed when pointing the laser beam. However, satellite rotation is not one of these. A target satellite rotating at 10 degrees/s at 500km would only cause a few μm repositioning error of the return beam on the laser station because photons spend only a few tens of ps inside the reflector elements, and beam pointing error due to satellite rotation is about 6 picoradians.

2.2. Thrust Plate to Control Nudging Laser Thrust Vector

Normally, thrust is perpendicular to the satellite surface, independent of the laser beam incidence angle. Fig. 3 shows a conceptual thrust plate composed of an array of ablative fuel hemispheres which can produce a thrust vector counter to the laser beam instead.

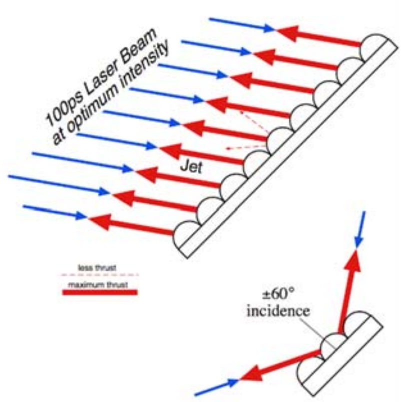

Fig. 3. Special Thrust Plate.

Note that we have not actually built and tested this device, but it will work as advertised if the laser intensity is tightly controlled to match the optimum ablation intensity at the surface normal of the thrust plate hemispheres. This device will have a 120° range of laser incidence angles using 100 ps pulses. This will allow us to better control target motion after impact of a high energy single laser pulse.

Nudging is done with a 0.1-1 kJ pulsed laser system similar to that in [3].

To be complete, we remind the reader that, with very high laser intensities, where plasma velocity v_p is relativistic, thrust can be tilted relative to surface normal without special arrangements (Fig. 4).

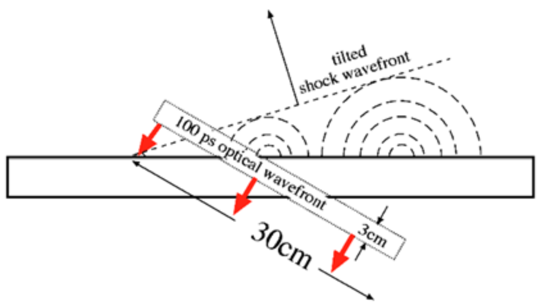

Fig. 4. Thrust vector with very hot plasmas can tilt relative to surface normal (angles exaggerated).

3. Chirped CW Laser

There is significant interest in using low power CW lasers (rather than 100 ps pulses) to locate debris in the JCA program. In this section, we will show that just 250 mW CW in a suitably "chirped" 1064 nm beam will provide adequate S/N at a range up to 500 km while locating targets within 1.5 cm.

Fig. 5 illustrates our laser pulse format. For this idea, we are indebted to a very well written thesis [7].

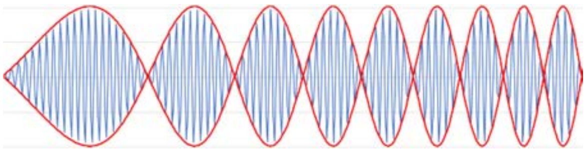

Fig. 5. Amplitude-modulated optical wave with chirped modulation frequency.

The Fig. 5 waveform is described by Eq. (1) with

$$E = \sin(\omega_1 t)\sin(\omega_2(1+bt)t) \qquad (1)$$

ω_1 the optical wave, and $\omega_2(1+bt)$ the linearly chirped amplitude modulation. We cannot perform direct operations on the optical wave without a complex optical interferometer. However, we can cross-correlate the returning (time-reversed) AM modulation pattern (shown in red) with a copy of that for the outgoing wave and select the peak to determine range.

Table 1 shows the numerical results for this system.

Table 1. Numerical results for CW laser ranging.

Wavelength	1064	nm
Mirror diameter	75	cm
M^2	1.5	
Max Target Range	500	km
Beam dia. on target	1.91	m
Search area dia. (solar illum	100	m
Laser pulse duration	10	ms
Laser power	250	mW
Chirp bandwidth	5	GHz
Corner reflector diameter	1	cm
Signal brightness at rcvr.	2.61	W/(m^2sr-um
Background brightness	2.70E-06	W/(m^2sr-um
S/N	9.70E+05	
Photodetector efficiency	70	%
S/dark current	6300	
Target location precision	1.5	cm
Precision interval (p.i.)	33	ps
Photoelectrons in p.i.	1310	
Quarter optical period T/4	50	ps
Phtoelectrons in T/4	1960	
Beat freq. at 500km	1.67	GHz

The optical frequency ω_1 is 282 THz. If we select b=500 GHz/s, the chirped modulation frequency covers a 5 GHz band and the spacial resolution c/(4B) =1.5 cm [8]. Chirped laser pulse duration is 10 ms at 250 mW at 1064 nm, giving a 2.5 mJ transmitted pulse energy. This precision is similar to our results with the 50 mJ, 100 ps pulsed laser source we discussed in [1] for ordinary satellite surfaces without corner reflectors.

Because of the frequency ramp, the return signal will exhibit a beat frequency when mixed with the outgoing signal (Fig. 6). For a stationary target, this freqency, f_B contains the range z. For range 500 km, the round trip delay 2 z/c is 3.33 ms, and the beat frequency will be 1.67 GHz.

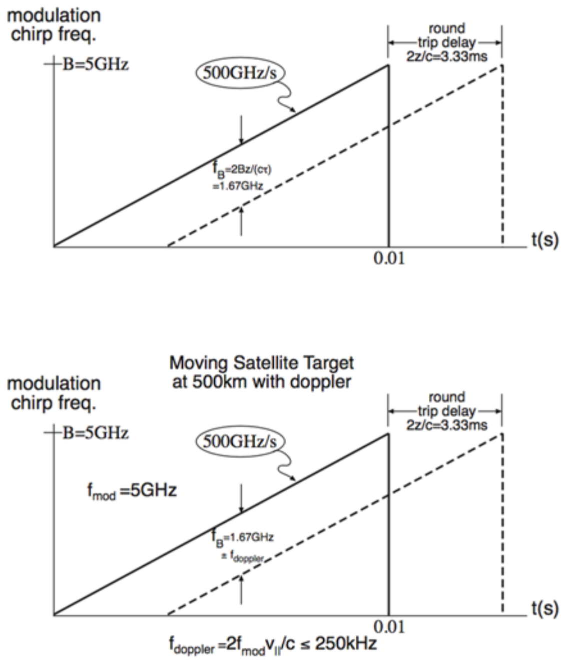

Fig. 6. Return signal with a) stationary and b) moving targets. The chirped pulse repeats every 10 ms.

However, if we consider a moving target with a 7.5 km/s velocity component parallel to the laser beam, f_B now contains an additional 250 kHz doppler component (Fig. 6b). To deal with this, three actions will be sufficient:

(1) Add one more modulation to the outgoing signal, consisting of many sharp (100 ps rise and fall), pseudo-randomly spaced dropouts;

(2) Because the target will have moved 75 m during the 10ms outgoing pulse, gradually stretching the return by 0.25 μs and ruining the possible precision, an onboard computer must recurrently estimate the Doppler frequency and add or subtract an onboard variable frequency oscillator signal from the recorded return until the best precision is obtained. We note that if this step is done perfectly, step 1) may not be necessary, but

we sugest to implement it because of the inevitable effects of noise;

(3) Cross-correlate the modified return with the stored transmitted signal.

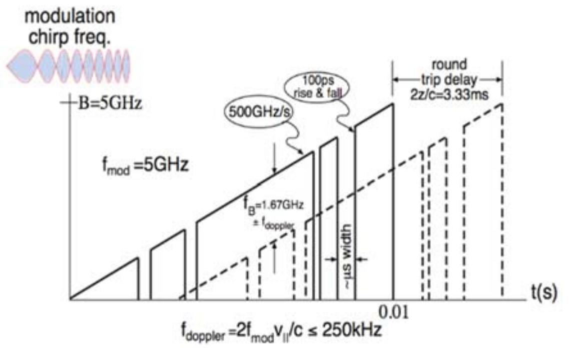

Fig. 7. Pseudo-random code modulation of outgoing signal.

Given these actions, we will obtain a single 100 ps pulse representing the target location with ±1.5 cm precision (Fig. 8).

4. Ranging Procedure

Fig. 9 shows the laser transmit/receive path. The ranging procedure is identical to that in [3], with the difference that the ranging signal is a 250 mW CW 1064 nm, 10 ms laser pulse. First, we find the target with a broad area search, using solar illumination of the target plane (yellow beam in Fig. 9).

Then, we aim the laser at the target and track it, obtaining its range in a few seconds. The telescope is designed to fit inside a Vega-C for launch.

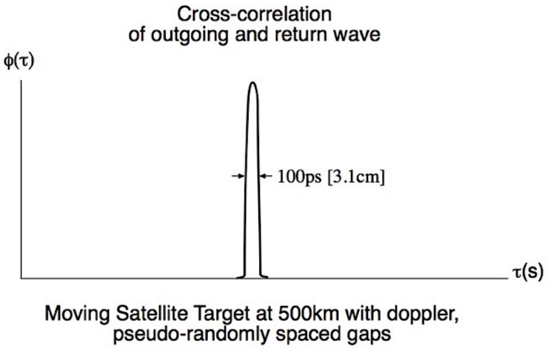

Fig. 8. Result of cross-correlating the outgoing and return signal with Doppler removed.

5. Laser

The laser follows closely the design of Li et al. [8], who achieved 400 Hz bandwidth in their single-frequency oscillator. See [8] for many additional details that are overlooked in the simplified block diagram in Fig. 10. In the Figure, a non-planar ring oscillator (NPRO) feeds an electro-optic modulator (EOM) which is input to a yttrium-doped fiber amplifier (YDFA) that produces 30W. The EOM is driven by a chirp signal generator with a DC bias control system.

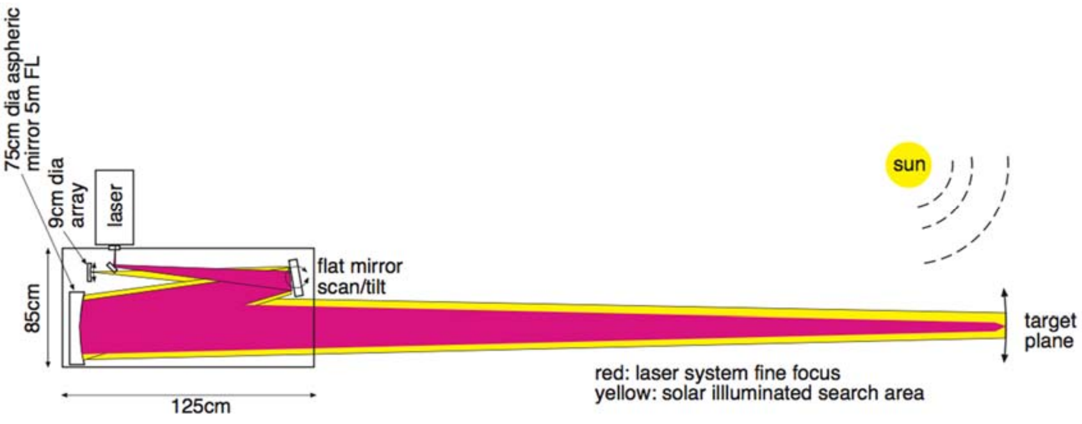

Fig. 9. Laser transmit/receive path to target, and array detector. Range is up to 500 km.

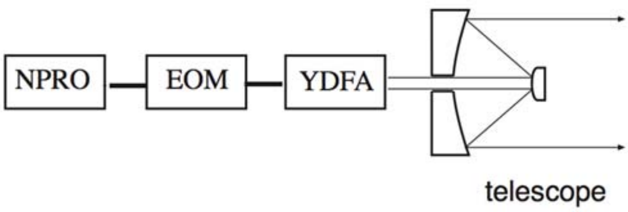

Fig. 10. Laser system block diagram.

6. Optimizing Kinetic Ablation Efficiency in Real Time using Thomson Scattering

Ablation efficiency is given by

$$\eta_{AB} = \Delta m v_i^2 / 2W = C_m v_i / 2 \quad (1)$$

with laser pulse energy W, momentum coupling coefficient C_m, ablated mass Δm and ion velocity v_i. We determine Cm from Δv_{target} in a single shot, as measured by the system described in §3. The novel approach we describe in this section is to measure ion velocity v_i using the Thomson scattering technique [9, 10], Fig. 11.

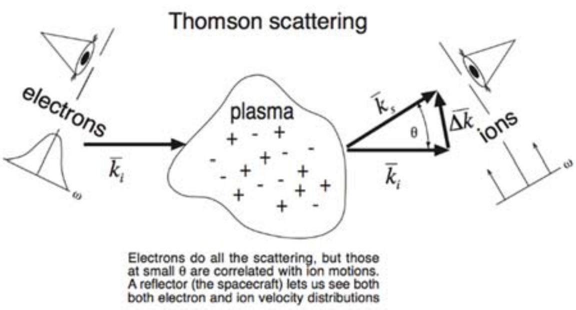

Fig. 11. Thomson scattering principle.

A short pulse laser provides wave vector $\mathbf{k_i}$. In Thomson scattering, the forward (collective scattering) direction gives the ion distribution. Where Δk is the scalar wave vector change and D_e is the electron Debye length, the Thomson scattering shape function in the limit $\alpha=1/(\Delta k D_e)>>1$ is

$$S(\Delta k,\omega) = Z\left|1+\frac{2T_e}{T_i}W(v/v_i)\right|^2 \frac{e^{-(v/v_i)^2}}{\sqrt{\pi}v_i}. \quad (2)$$

for a maxwellian plasma, but the technique will give the actual velocity distribution if the plasma is non-maxwellian. In Eq. (2), Z is ion charge state and W is an integral described in [9]. In the backward direction, the electron velocity distribution is given, but we want the ion distribution here. Fortunately, the satellite itself reflects the ion feature back to us. Now, the parameters in Eq. (1) are available to us and we can dither pulse energy W until η_{AB} is maximum. The ion feature is easily distinguished from the electron feature because it is very close to the laser frequency.

7. How to Avoid Melting Propelled Targets

This section, and the one following, refer to an entirely different scenario in which intense, repetitive short pulses (of order 100 ps) are used to propel a space object. Ref. [11] showed that the maximum pulse number to avoid melting can be written

$$N_{max}=(2/3)^{1/3}C_pM(T_m-Ti)/(C_{th}W) \quad (3)$$

With M indicating target mass, T_m and T_i the melting and initial temperatures, C_{th} the thermal coupling coefficient and W the laser pulse energy. This relationship assumes we heat the entire ablation fuel block, and limits us to about 2,000 pulses for a few-kg aluminum target. In [11], it was stated that a few-kg aluminum debris could not be re-entered without a cooldown. Further, many flights that have been proposed need hundreds of thousands of pulses [13]. There is a solution to this problem: at very high laser intensity on target, surface recession will outrun the thermal wave. If we apply high intensity plasma theory[12], we can achieve conditions in which $v_{rec}/v_{th}>>1$, as shown in Eq.(4):

$$v_{rec}/v_{th} = 1.26E-6\frac{A^{7/8}}{\tau^{0.75}[Z^2(Z+1)]^{3/8}}\sqrt{\frac{\Phi}{\lambda\rho}} \quad (4)$$

In Eq. (4), Φ is fluence (J/m^2), A is average atomic mass number in the plume, Z is average ionic charge, λ is wavelength, K is thermal conductivity of the solid fuel ρ is the solid fuel density (kg/m^3) and τ is laser pulse duration. With typical values for laser space flights (355 nm, 100 ps, 40 kJ/m^2), and properties of calcium silicate, Eq.(4) gives $v_{rec}/v_{th}=3.2\text{x}10^6$.

8. A Figure of Merit for Ablation Fuels

We suggest a figure of merit for long laser ablation flights as shown in Eq. (5):

$$FOM = \frac{\eta_{AB}T_m}{C_{th}K} \quad (5)$$

This figure of merit emphasizes ablation efficiency and melting temperature, and de-emphasizes thermal coupling coefficient C_{th} and thermal conductivity. Ablation efficiency and C_{th} have not been measured for all materials, but estimates give the results in Table 2, which shows how important refractory materials (rather than low melting metals) will be for ablation fuels in future laser propelled flights.

Table 2. Figure of merit for several ablation fuels.

Matl	EtaAB	Tm	K	Cth	FOM
Fiberglas	0.2	1120	0.04	0.3	1.87E+04
Ca2SiO4	0.2	2130	0.2	0.3	7.10E+03
ZrO2	0.2	2715	1.7	0.3	1.06E+03
CaCO3	0.2	2072	2.25	0.3	6.14E+02
Zr	0.6	3371	16.7	0.3	404
POM	0.2	175	0.31	0.3	376
SiC	0.2	3545	39	0.3	61
Al	0.22	660	239	0.03	20
WC	0.2	2870	110	0.3	17
Graphite	0.06	3600	470	0.15	3.1
	Estimates for materials not measured				

A brief presentation of this work was given as an oral paper in [14].

9. Conclusions

In this paper, we have outlined two preflight actions which will improve laser ranging, a procedure which will permit using a 250 mW CW laser for ranging, and a method to optimize kinetic efficiency in the nudging operation. We also discussed a way to partially control thrust direction and a way to search for better ablation fuels which can take many more than 2,000 pulses before melting.

Acknowledgments

We gladly acknowledge Prof. Sergey Yurish for providing a path to publication for this work, and for his effort in setting up OPAL' 2022.

References

[1]. C. Bonnal, D. McKnight, C. Phipps, C. Dupont, S. Missonier, L. Lequette, M. Merle and S. Rommelaere, Just in time collision avoidance – a review, *Acta Astronautica*, 170, 2020, pp. 637-651.

[2]. C. Phipps and C. Bonnal, A spaceborne, pulsed UV laser system for re-entering or nudging LEO debris, and re-orbiting GEO debris, *Acta Astronautica*, 118, 2016, pp. 224-236.

[3]. C. Phipps, L'ADROIT – A spaceborne ultraviolet laser system for space debris clearing, *Acta Astronautica*, 104, 2014, pp. 243-255.

[4]. S. Somerstein, J. Fuller and R. Kennedy, Retroreflector field of view properties for open and solid cube corners, *SPIE Proceedings*, 1168, 1989.

[5]. J.-M. Gambi, C. Phipps, M. L. Del Pino, M. C. Rodriguez-Teijeiro and J. I. Arana, Post-Newtonian Corrections to JCA, Paper 6.2, in Proceedings of the *6th Workshop on Space Debris Modeling and Remediation*, Politecnico Milano, Italy 18-20 May, 2022.

[6]. J. M. Gambi and M. L. Garcia del Pino, Post-Newtonian tracking formulae to increase the shooting accuracy of autonomous LEO laser trackers, *Adv. in Space Research*, 67, 2021, pp. 2282-2303.

[7]. P. Adany, Simplified homodyne detector for FM chirped lidar, B. S. Thesis, *University of Kansas*, 2007.

[8]. S. Li, S. Yang, Z. Wang and Z. Li, High-power broadband-chirped intensity-modulated single-frequency 1064 nm laser, *Appl. Sci.*, 10, 2020, 4450.

[9]. C. Phipps and D. Bershader, Measurement of nonisotropic electron velocitiy distributions by laser scattering, in Dynamics of Ionized Gases, M. J. Lighthill, I. Imai and H. Sato (Eds.), *University of Tokyo Press*, 1973.

[10]. M. Kaloyan, S. Ghazaryan,C. Constatantin, R. Post, P. Heuer, J. Pilgram, D. Schaeffer and C. Nieman, Raster Thomson scattering in large-scale laser plasmas produced at high repetition rate, *Rev. Sci. Inst.*, 92, 2021, 093102.

[11]. S. Scharring, R. Lorbeer and H.-A. Eckel, Heat accumulation in laser-based removal of space debris, *J. AIAA*, 56, 2018, pp. 2506-2508.

[12]. C. Phipps, T. Turner, R. Harrison, G. York, W. Osborne, G. Anderson, X. Corlis, L. Haynes, H. Steele, K. Spicochi and T. King, Impulse Coupling to Targets in Vacuum by KrF, HF and CO_2 Lasers, *J. Appl. Phys.*, 64, 1988, pp. 1083-1096.

[13]. C. Phipps, C. Bonnal, F. Masson, M. Boustie, L. Berethe, M. Schneider, S. Baton, E. Brambrink, J.-M, Chevalier, L. Videau and S. A. E. Boyer, Transfers from Earth to LEO and LEO to interplanetary space using lasers, *Acta Astronautica*, 146, 2018, pp. 92-102.

[14]. C. Phipps and C. Bonnal, Preparing Satellites for Active Debris Removal and Ranging, in *Proceedings of the 5th International Conference on Optics, Photonics and Lasers (OPAL' 2022)*, 2022, pp. 48-50.